

Ultrafast X-ray computed tomography for phase distribution and velocity measurements in multiphase flows

Martina Bieberle^{1,*}, Michael Wagner¹, Frank Barthel², Swapna Rabha², Manuel Banowski²,
Uwe Hampel^{1,2}

¹ Technische Universität Dresden, AREVA Endowed Chair of Imaging Techniques
in Energy and Process Engineering, 01062 Dresden, Germany

² Helmholtz-Zentrum Dresden – Rossendorf, Institute of Fluid Dynamics,
Bautzner Landstraße 400, 01328 Dresden, Germany

*corresponding author: martina.bieberle@tu-dresden.de

Abstract Various flow measurement and visualization techniques are based on optical and laser-based methods. However, in many multiphase flow situations, e.g. at higher interfacial density or in flows with internals, the optical access is no longer given. Radiation based methods are in principle able to penetrate most of these systems, but are normally too slow to capture the dynamics of the flow. With ultrafast X-ray tomography a flow visualization and measurement technique has been developed, which is able to recover the dynamic phase distributions in various multiphase flow scenarios. The high imaging rate is achieved by deflecting an electron beam along a circular target, where a moving X-ray spot is generated. Tomographic projections are gathered simultaneously by a static detector ring with fast read-out. Thus, no components of the X-ray tomography system have to be rotated mechanically. The reconstructed tomography slices represent the non-superimposed phase distribution within a cross-section as a function of time. Up to 8,000 fps can be achieved in single plane mode. For velocity measurements, a second set of X-ray target and detector ring arranged at a small axial distance can be included to form the so-called dual plane mode. Although the alternating scanning of both planes reduces the frame rate by a factor of two, the benefit of combining the information from both planes to retrieve velocity information arises directly. There are different ways to extract velocity information from the two stacks of slice image data. Cross-correlation techniques offer the opportunity to retrieve time averaged as well as time resolved local or global velocities of the disperse phase. Some systems also allow the determination of single bubble or particle velocities, provided that they can be identified as the same object in both planes.

Keywords: ultrafast, X-ray CT, multiphase flows, velocity, phase distribution

1 Introduction

Multiphase flows are characterized by the presence of two or more distinct phases, which influence each other across the phase boundary in different ways. Beside momentum transfer among the phases as a results of pressure differences and gravitational forces; chemical reaction, addition of internal and external heat source and concentration gradient influence the phase distribution. As a result, the heat and mass transfer among the phases and finally overall performance of the system get affected. The variety of beneficial multiphase flows in chemical engineering, mineral oil processing and power engineering leads to the need of enhanced investigations reaching from understanding the fundamental physics to the optimization of existing industrial facilities.

Since optical access is limited in some flow situations such as in the presence of opaque materials as process media or container or flow regimes with high interfacial density, tomographic techniques have gained growing interest in the last decades. Although classical X-ray tomographic techniques are quite slow, they at least enable imaging of stationary parts of the flow [1]. In order to find faster alternatives, different kinds of electrical tomography techniques were developed. Electrical impedance tomography (EIT) [2] and electrical capacitance tomography (ECT) [3] are comparably cheap and can reach frame rates of several thousand per second, but are strongly limited in spatial resolution to about one tenth of the object diameter. This situation led to the need of more sophisticated tomography techniques for flow imaging, one of which is the ultrafast electron-beam X-ray computed tomography. This technique was developed at the Helmholtz-Zentrum Dresden – Rossendorf [4] and has been applied to various two- and three-phase flow experiments, e.g. gas-liquid flow in vertical pipes [5], bubble and slurry bubble columns [6], gas-liquid flow in monolith or ceramic foam structures, static mixers [7], separators and impellers, as well as gas-solid fluidized beds [8] and spout fluidized beds.

2 Ultrafast X-ray computed tomography

Computer tomographic (CT) imaging is based on acquiring projection data of the object of interest from different angular views and reconstructing the non-superimposed structure of the object by solving the corresponding inverse problem. In order to speed up the data acquisition for flow visualization, the principle of electron beam X-ray tomography is exploited in this ultrafast X-ray CT system [9] (Figure 1). There, an electron beam is focused onto a heavy metal target, where it induces the generation of X-ray radiation. By electromagnetically deflecting the electron beam along the ring-shaped target a rapidly moving X-ray source spot is generated. The corresponding detector elements are arranged on a ring around the object of interest. Thus, no mechanically moving components are required for this measurement technique. With the fast read-out capability of the detector of $f_{\text{Det}} = 1$ MHz, this ultrafast CT system is able to acquire projection data from multiple positions per electron beam revolution according to $N_p = f_{\text{Det}}/f_{\text{Sou}}$, wherein f_{Sou} is the deflection frequency of the electron beam. Since the latter corresponds to the final frame rate, a compromise between temporal and spatial resolution must be found for each application. The frame rate can be chosen between 500 and 8000 images per second, whereas the number of available projections N_p per image follows as 125 to 2000.

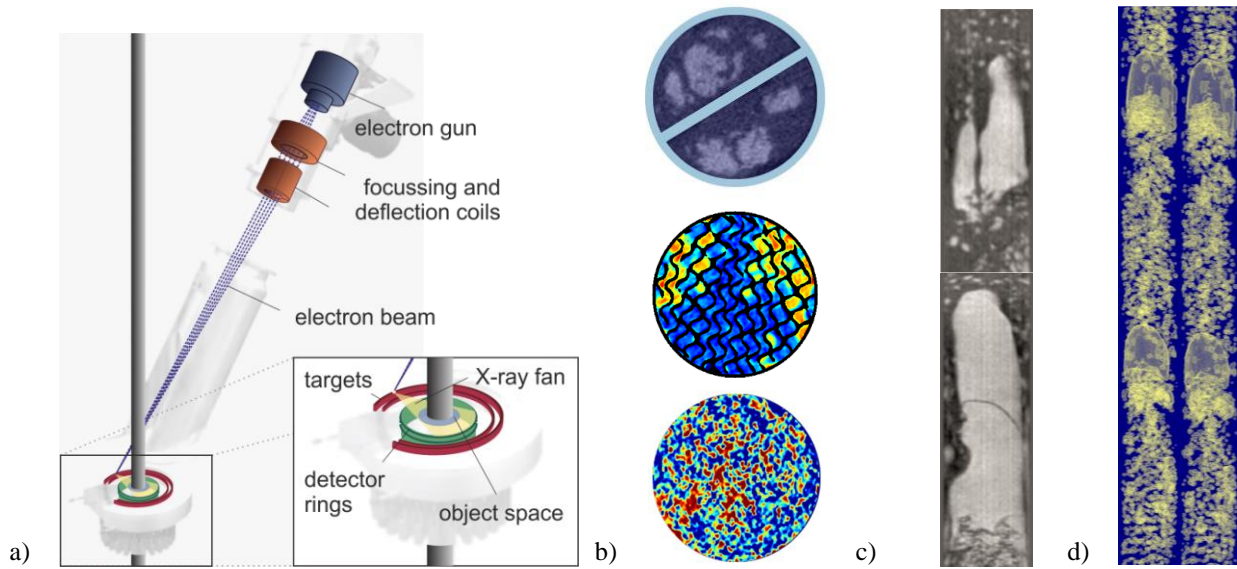


Figure 1: Principle of ultrafast X-ray CT (a), sample images of gas-liquid flows within structures (static mixer, structured packing, ceramic foam) (b), virtual side view of gas-liquid pipe flow indicating interesting details (small bubbles beside and in the wake of large bubbles and water lamellae between bubbles) (c), 3D view of pipe flow image sequences from both CT planes (d).

A further option of the ultrafast X-ray CT system is its dual plane mode. The combination of X-ray source target and detector ring is installed twice with a defined distance in axial direction. The electron beam is guided alternately along both targets to achieve quasi simultaneous imaging in both planes. Thus, also information about the axial velocity of moving structures within the object of interest can be retrieved in addition to the material distribution. For multiphase flow analysis this is especially important, since the true dimensions in axial direction can only be retrieved from the image sequence, if the velocity of the current object is known, which is in general not the case.

3 Image reconstruction

The forward problem of transmission tomography can be described by the Radon transform

$$p(s, \theta) = \int_{-\infty}^{+\infty} \int_{-\infty}^{+\infty} \delta(s - x \cos\theta - y \sin\theta) \mu(x, y) dx dy. \quad (1)$$

Therein, $\mu(x, y)$ is the unknown distribution of the linear X-ray attenuation coefficient within the object of investigation, $p(s, \theta)$ is the measured attenuation data and the parameters s and θ characterize each ray path by its distance from the origin of the x, y - coordinate system and its inclination, respectively. The attenuation p is derived from the measured intensities with (I) and without object (I_0) according to the Beer-Lambert law as

$$p = -\ln\left(\frac{I}{I_0}\right). \quad (2)$$

One way to solve the inverse problem is given by the filtered back projection algorithm. The unknown object distribution can be recovered by

$$\mu(x, y) = \int_0^{\pi} \int_{-\infty}^{+\infty} h(s)p(s, \theta) \cdot \delta(s - x \cos\theta - y \sin\theta) ds d\theta \quad (3)$$

with $h(s)$ being a filter function correcting the error arising from the approximation of the simple back projection. Beside the ramp filter as the correct filter function by theory, derivatives like the Hamming or Shepp-Logan filter [10] are proven to be suitable alternatives in practical applications with noisy measurement data.

Another way of formulating the tomography problem is a linear equation system of the form

$$\mathbf{p} = \mathbf{A} \cdot \boldsymbol{\mu}. \quad (4)$$

The vectors \mathbf{p} and $\boldsymbol{\mu}$ include all values resulting from a discretization of $p(s, \theta)$ and $\mu(x, y)$, respectively, and the matrix \mathbf{A} maps the values from $\boldsymbol{\mu}$ to \mathbf{p} according to the geometrical interrelation described in (1). Various approaches have been pursued in order to solve the equation system (4). One iterative technique is the so called algebraic reconstruction technique (ART). In each iteration, one equation corresponding to one ray path is solved according to

$$\boldsymbol{\mu}^{(i+1)} = \boldsymbol{\mu}^{(i)} + \lambda \frac{p_k - \mathbf{a}_k \cdot \boldsymbol{\mu}^{(i)}}{\|\mathbf{a}_k\|^2} \mathbf{a}_k^T, \quad (5)$$

wherein λ is a relaxation factor for steering the convergence of the algorithm. Although there might be no unique solution for the equation system in the presence of noisy data, it has been shown that the algorithm converges towards the minimum norm solution of (4).

Both of the described reconstruction techniques as well as a specialized reconstruction technique for binary distributions based on the level set method [11] are implemented for the described measurement technique.

4 Data analysis

The analysis of ultrafast X-ray CT image sequences comprises four major categories, namely image preprocessing, phase segmentation, feature extraction and velocity determination. The exact way of applying these data analysis tools depends on the kind of application. In this section, an overview of available routines is given while in section 5 different examples of multiphase flow experiments with selected results are presented.

The reconstructed image sequences $\mu_A(x, y, t)$ and $\mu_B(x, y, t)$ from the two imaging planes A and B, respectively, are preprocessed by selectable steps from a set of preprocessing routines including noise reduction by median filtering, position correction for moving or vibrating objects, intensity correction for periodic disturbing signals and scatter correction [12]. Furthermore, a normalization step based on scaling between the values of single phase references is required in general. For example, the gas fraction ε_G distribution of a two-phase flow can be calculated on the basis of the gas and liquid reference

measurements μ_G and μ_L , respectively, as

$$\varepsilon_G(x, y, t) = \frac{\mu_L(x, y) - \mu_I(x, y, t)}{\mu_L(x, y) - \mu_G(x, y)}. \quad (6)$$

After preprocessing, the data sets are generally denoted as $\mu'_I(x, y, t)$ with $I \in \{A, B\}$.

For the investigation of multi-phase flows, the next step is in general the segmentation of the two or more phases present in the object of investigation. Depending on the distinct application, several algorithms from simple thresholding to advanced level-set segmentation are available. For the most frequent case of gas bubbles within a continuous liquid, a specialized segmentation algorithm based on the agglomeration of pixels for each bubble has been developed and validated by global measures [13]. The result of this segmentation algorithm is a data set $b_I(x, y, t)$ of the same size as the original image data set $\mu'_I(x, y, t)$ indicating the bubble identification number for each of its voxels.

On the basis of the data sets $b_I(x, y, t)$ and $\mu'_I(x, y, t)$, different feature extraction algorithms can be applied. Parameters, which are most often of interest, are radial phase fraction profiles, cross-section averaged phase fraction sequences and bubble size distributions as well as spatial bubble distributions. While calculating radially, time or cross-section averaged parameters is quite straight forward, information about bubble or phase boundary velocities in axial direction are necessary to determine bubble sizes. Ways of obtaining velocities out of the image sequences from the two measurement planes are described below.

In pipe or column flow with stationary velocity distribution, a time-independent velocity distribution or even radial velocity profile will be sufficient. Both can be determined by applying the cross-correlation function

$$\Psi_{AB}(x, y, \tau) = \frac{1}{T - |\tau|} \begin{cases} \sum_{t=0}^{T-1-\tau} \mu_A(x, y, n) \cdot \mu_B(x, y, (t + \tau)) & \text{for } \tau \geq 0 \\ \sum_{t=-\tau}^{T-1} \mu_A(x, y, n) \cdot \mu_B(x, y, (t + \tau)) & \text{for } \tau < 0 \end{cases} \quad (7)$$

between planes A and B and then calculating velocities $v(x, y)$ by dividing the distance of the measurement planes by the τ with the highest value of $\Psi_{AB}(x, y, \tau)$ for each x and y . The window size T corresponds to the number of frames in the sequence in this case. Theoretical, it is also possible to create a time dependent analysis by reducing the window size T . However, this is limited because the reliability of maximum cross correlation value decreases drastically with smaller window size. The best way to determine the axial velocity for each object (e.g. bubble) would be to identify the object in both planes and derive its velocity from the corresponding temporal offset. Although this identification step is not trivial due the correspondence problem of the very similar objects, an algorithm has been derived [14], which takes the mean fluid velocity, the object size and its in-plane position as mature probability density functions into account. At best conditions, an assignment rate of around 90 % is achieved.

5 Examples of multiphase flow measurement

5.1 Gas-liquid flow in vertical pipe

Multiphase flow in pipes is part of many industrial plants, especially power plants, but plays also an important role in chemical industry and mineral oil production. To improve the general understanding of two-phase flow in vertical pipes and support the development of new models for multiphase computational fluid dynamics (CFD), large scale experiments have been performed at HZDR covering a wide range of flow parameters. The results presented here originate from experiments within a DN50 titanium pipe with a height of 6 m. Inlet parameters, i.e. gas and liquid superficial velocities, J_G and J_L , respectively, have been varied in order to cover all flow regimes from bubbly to annular flow. Details can be found in [5]. Figure 2 shows selected results in form of virtual side views of the phase boundary together with derived radial profiles of gas fraction and axial velocity. Note, that the vertical axis of the images represents time. Thus, the images show the temporal evolution of the ε within the CT cross section.

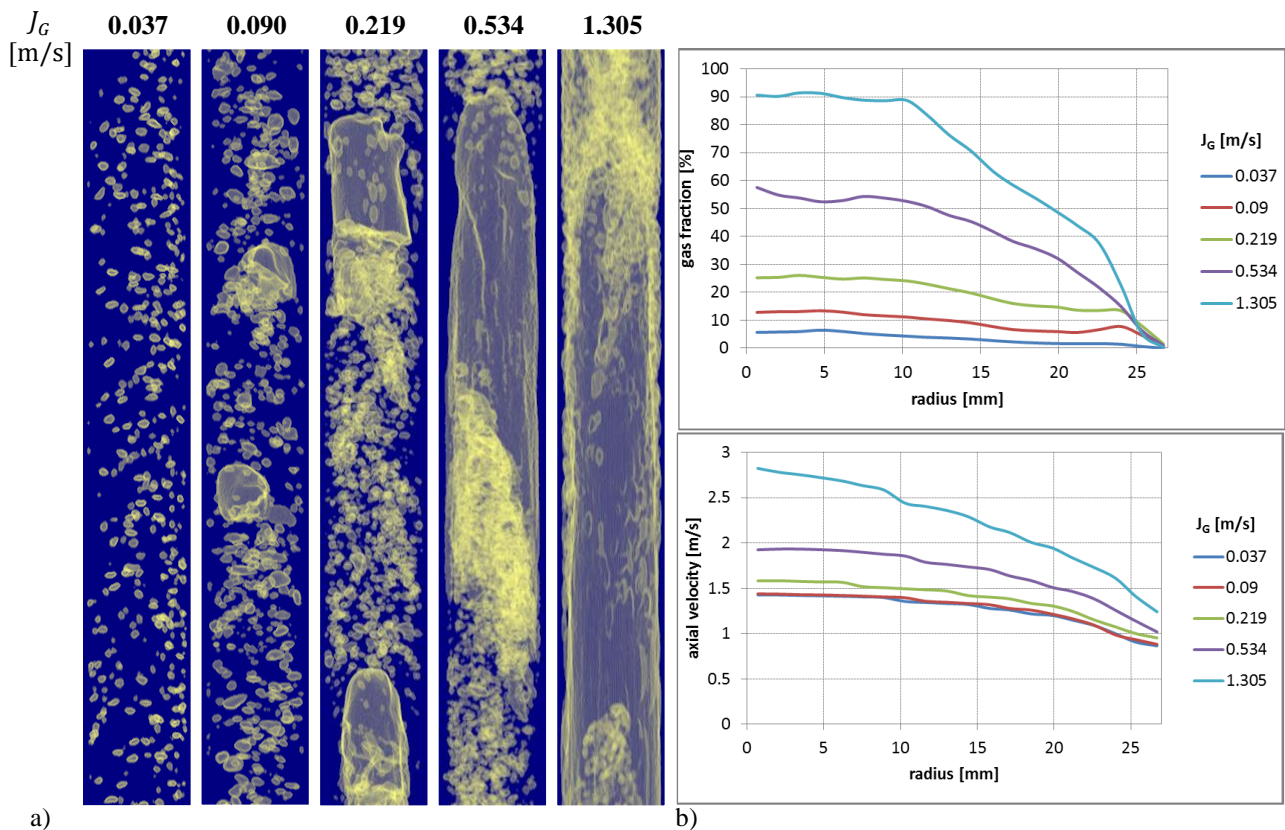


Figure 2: X-ray CT results of vertical air-water pipe flow experiments: Virtual side views of the phase boundary (left) and radial profiles of gas fraction and axial velocity (right) for different superficial gas velocities J_G at a superficial liquid velocity of $J_L = 1.017$ m/s.

As can be seen from the virtual side views, the structure of the phase boundary can be resolved in very detail despite axial flow velocities of more than 1 m/s. The flow regime is clearly perceivable as well as various smaller scale hydrodynamic phenomena, for example the dynamics of small bubbles behind large Taylor bubbles in the slug flow regime. Beside those qualitative results, the quantitative results in form of radial profiles provide valuable information for the validation of CFD codes by comparing the experimental results with those from simulations.

5.2 Bubble and slurry bubble columns

Bubble column reactors are widely used for industrial chemical reactions. Since both the interfacial density and the pressure drop are not yet optimal with respect to mass transfer and energy consumption, respectively, this type of reactor is still subject to research. Furthermore, the slurry bubble column (SBC) reactor is of special interest, since it is proven to be the best reaction device for Fischer-Tropsch processes [15], which in turn are currently in the focus of worldwide research due to their ability of converting remote natural gas to liquid transportation fuels. Therefore, the influence of the solid concentration c_s of spherical glass particles ($d_p = 100 \mu\text{m}$) on the hydrodynamics within a 70 mm diameter bubble column has been investigated using ultrafast X-ray CT. The revealed structures are presented in Figure 3. Although the shape of the bubbles cannot be directly perceived in the sequence plot due to their different velocities, the main structure of the flow can be observed and bubble sizes can be derived either by determining their velocities between the two measurement planes (large bubbles) or from the 2D images by assuming elliptical shapes (small bubbles). The main effect of the added particles was an increased bubble coalescence leading to a decreased cross-section gas hold-up. This effect increased with particle concentration except for very high concentrations, where large bubbles started to break up again. Further details can be found in [6].

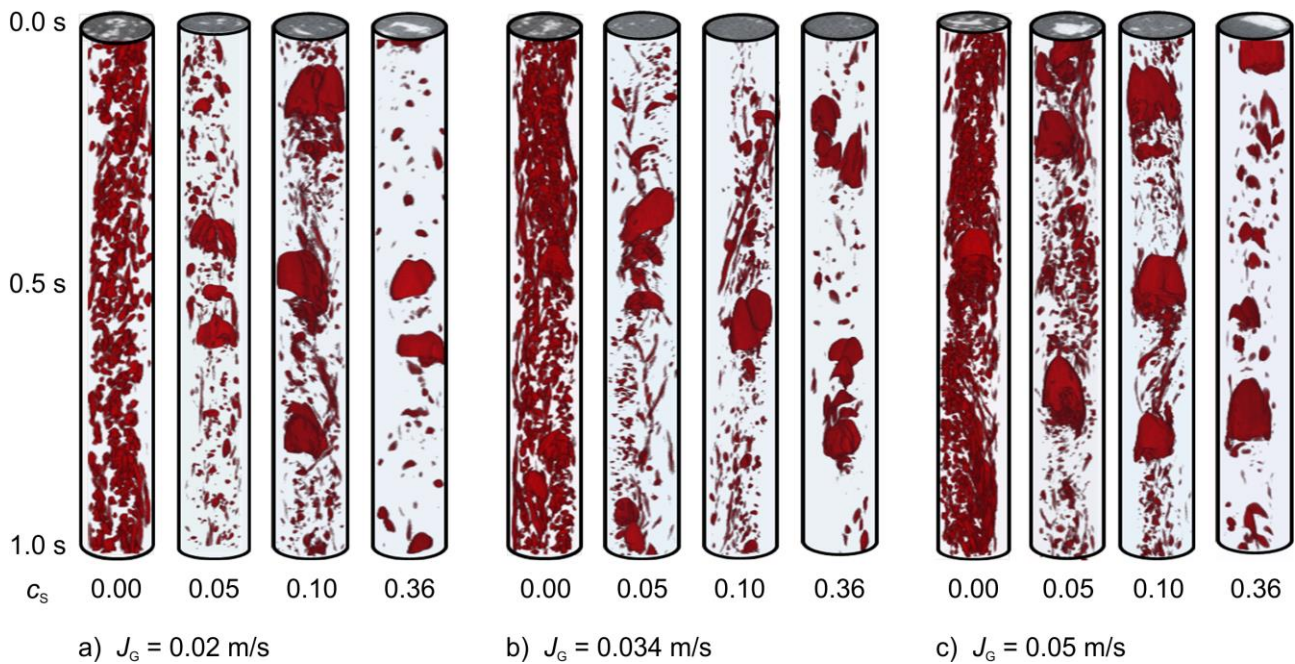


Figure 3: 3D-plots of image sequences of bubble and slurry bubble column at different superficial velocities (J_G) and solid particle concentrations (c_s).

5.3 Fluidized beds

Gas-solid two-phase flows occur in different forms in several industrial branches. The fluidized bed as one of these forms has for example applications in chemical reaction, combustion, drying, granulation and coating. The basic principle of fluidized bed is to create a process with high surface area and good mixing conditions for optimal heat and mass transfer by applying a gas flow from the bottom into a particle bed. Although there exists quite a lot of experience on the operation of fluidized beds, the complete physics is not yet understood in the detail, which would be necessary to simulate the whole dynamics of fluidized beds for different conditions. Therefore, great effort is spent on studying its behavior in experiments. However, due to the mostly dense distribution of opaque media in fluidized beds, measuring the particle distribution is a challenging task. Here, ultrafast X-ray CT was applied to an experimental fluidized bed of 1 mm diameter glass beads with initial height of 200 mm within a 100 mm diameter column. The phase distribution within the measuring planes was recovered at a frame rate of 1000 images per plane per second for gas inlet velocities J_G in the range of $1.25 J_{mf} \leq J_G \leq 2.0 J_{mf}$ with J_{mf} being the minimum fluidization velocity. A sketch of the principle setup and resulting X-ray images are shown in Figure 4. The cross-sectional as well as virtual axial slice images show the material distribution for the different gas inlet velocities. It is obvious, that the revealed structures are more complex than in gas-liquid systems, where a clear phase boundary defines bubbles, droplets or at the very most streaks. Here, dense, dilute and void regions merge into one another without a defined boundary in between and form structures, which could be described as bubbles, streaks, curtains or other forms of dense or dilute regions. Taking only the large bubble structures into account, the X-ray CT results have been compared with simulations based on the two-fluid model [16]. More detailed analysis of the X-ray CT data is subject to ongoing research.

References

- [1] Viva A, Aferka S, Brunazzi E, Marchot P, Crine M, Toye D (2011). Processing of X-ray tomographic images: A procedure adapted for the analysis of phase distribution in MellapakPlus 752.Y and Katapak-SP packings. *Flow Measurement and Instrumentation*, vol. 22, pp. 279–290.
- [2] York T (2001) Status of electrical tomography in industrial applications, *Journal of Electronic Imaging*, vol. 10, pp. 608–619.
- [3] Marashdeh Q, Fan L-S, Du B, Warsito W (2008) Electrical Capacitance Tomography – A Perspective, *Industrial & Engineering Chemistry Research*, vol. 47, pp. 3708-3719.
- [4] Fischer F, Hampel U (2010) Ultra fast electron beam X-ray computed tomography for two-phase flow measurement, *Nuclear Engineering and Design*, vol. 240, pp 2254–2259.
- [5] Lucas D, Banowski M, Hoppe D, Beyer M, Szalinski L, Barthel F, Hampel U (2012) Experimental data on vertical air-water pipe flow obtained by ultrafast electron beam X-ray tomography measurements, Proc. of CFD4NRS-4, The Experimental Validation and Application of CFD and CMFD Codes in Nuclear Reactor Technology, 10.-12.09.2012, Daejeon, Korea
- [6] Rabha S, Schubert M, Wagner M, Lucas D, Hampel U (2013) Bubble size and radial gas hold-up distributions in a slurry bubble column using ultrafast electron beam X-ray tomography. *AIChE Journal*, vol. 59(5), pp 1709–1722.
- [7] Rabha S, Schubert M, Grugel F, Banowski M, Hampel U (2015) Visualization and quantitative analysis of dispersive mixing by a helical static mixer in upward co-current gas–liquid flow. *Chemical Engineering Journal*, vol. 262, pp 527–540.
- [8] Bieberle M, Barthel F, Hampel U (2012) Ultrafast X-ray computed tomography for the analysis of gas-solid fluidized beds, *Chemical Engineering Journal*, vol. 189-190, pp 356-363.
- [9] Barthel F, Hoppe D, Banowski M, Beyer M, Lucas D, Hampel U (2014) Non-Invasive Two Phase Pipe Flow Imaging Using Ultrafast Electron Beam X-ray Tomography, *Nuclear Engineering and Design* (submitted).
- [10] Kak A C, Slaney M (1988) Principles of Computerized Tomographic Imaging. IEEE Press, New York.
- [11] Bieberle M, Hampel U (2015) Level-set reconstruction algorithm for ultrafast limited angle X-ray computed tomography of two-phase flows, *Philosophical Transactions of the Royal Society A*, vol. 373, 20140395.
- [12] Wagner M, Barthel F, Zalucky J, Bieberle M, Hampel U (2015) Scatter analysis and correction for ultrafast X-ray tomography, *Philosophical Transactions of the Royal Society A*, (accepted).
- [13] Banowski M, Lucas D, Szalinski L (2015) A new algorithm for segmentation of ultrafast X-ray tomographed gas-liquid flows. *International Journal of Thermal Sciences*, vol. 90, pp 311–322.
- [14] Patmonoaji A, Banowski M, Lucas D, Deendarlianto (2013) Investigation of gas bubble velocities from experimental data of ultrafast two-layer electron beam X-ray tomography. In: Proceeding of the 12th Annual National Seminar of Mechanical Engineering (SNTTMXII) October23rd-24th. Bandar Lampung, Indonesia.
- [15] Krishna R, De Swart JWA, Ellenberger J, Martina GB, Maretto C (1997) Gas holdup in slurry bubble columns: effect of column diameter and slurry concentrations, *AIChE Journal*, vol. 43(2), pp 311–316.
- [16] Verma V, Padding J T, Deen N G, Kuipers J A M, Barthel F, Bieberle M, Wagner M, Hampel U (2014) Bubble dynamics in a 3-D gas–solid fluidized bed using ultrafast electron beam X-ray tomography and two-fluid model, *AIChE Journal*, vol. 60(5), pp 1632–1644.